JOURNAL OF MATERIALS SCIENCE **37** (2002) 1967–1972

Oxygen condensation stacking faults in crystallized Co found during magnetic annealing of Co-rich amorphous alloy

H. KYUNG, C. S. YOON, C. K. KIM*
Department of Materials Science and Engineering, Hanyang University, Seoul, 133-791, Korea
E-mail: ckkim@hanyang.ac.kr

Amorphous $Co_{75.26-x}Fe_{4.74}(BSi)_{20+x}$ ($0 < x$) magnetic alloys were examined with Transmission Electron Microscopy (TEM) after magnetic field annealing. TEM analysis revealed that the crystallized Co layer under the surface oxide could be highly faulted with planar defects depending on the composition. Based on the electron diffraction, we have proposed a new form of stacking fault in which two oxygen atoms are substituted for FCC Co in the {111} planes to create randomly distributed clusters of oxygen atoms on the Co {111} planes. Such clusters would explain the absent {200} peak in the highly faulted composition of crystallized FCC Co and the streaks observed in the electron diffraction pattern of the material. The oxygen fault was also closely related to the magnitude of the induced magnetic anisotropy of the material, suggesting the Co–O bonds acting as the localized antiferromagnetic region.

1. Introduction

Soft magnetic materials produced through rapid solidification technology represent an unique class of magnetic materials characterized by high permeability, high B-H loop squareness and low coercivity [1]. In addition to the excellent magnetic properties, the hysteresis loop of the glassy materials can be easily tailored by annealing in an external magnetic field and inducing a magnetic anisotropy within the cast strip [2]. Out of the recently developed metallic glass systems, the Co-based alloys exhibit the best soft magnetic properties with near zero magnetostriction, which renders the material a potential candidate for host of industrial applications including magnetic recording head and electronic security sensor [3–6].

Our previous microstructure study of the $Co_{75.26-x}Fe_{4.74}(BSi)_{20+x}$ ($0 < x < 5$) magnetic strips showed that during the field annealing process at temperatures below its bulk crystallization temperature, the Co-based amorphous alloy will develop a complex layer of microstructures depending on the composition and annealing temperature [7]. The magnetic properties of the annealed strips were dictated by the resulting microstructure of the film. One of the distinguishing features in the microstructure was the high density of planar defects found in the crystallized FCC Co layer underneath the surface oxide of the film. As the density of the faults was closely linked to the magnitude of the exchange anisotropy found in the material [8], it is of great importance to identify the source of such defect in order to tailor the magnetic properties of the material as desired.

In this study, Transmission Electron Microscopy (TEM) was used to provide crystallographic evidence for the nature of the fault found in the crystallized Co layer.

2. Experimental procedure

Amorphous $Co_{75.26-x}Fe_{4.74}(BSi)_{20+x}$ for $0 < x$ alloy films were produced by planar flow casting at the Metglas Products Division of Allied-Signal Corporation, Parsippany, NJ.

Typical samples produced were 20 μm thick and 3 mm wide. Supplied compositions of the samples were verified by chemical analysis with X-ray photoelectron spectroscopy (XPS) and Energy Dispersive Spectroscopy (EDS) and the agreement was within the experimental error.

Differential scanning calorimetry (DSC) was used to determine the crystallization temperature. DSC indicates that the onset of the crystallization of amorphous $Co_{75.26-x}Fe_{4.74}(BSi)_{20+x}$ occurs at 465°C with its maximum peak at 535°C. Magnetic field annealing was done below its crystallization temperature in a longitudinal magnetic field of 60 Oe.

Transmission Electron Microscope (TEM, JEOL 2010) was used to study the microstructural detail of the Co-rich amorphous alloy. To prepare the TEM specimen, an ion mill was used to thin the sample to the

*Author to whom all correspondence should be addressed.

desired depth using a liquid-nitrogen cooled cold stage to ensure minimal heating of the sample during milling.

3. Results

Shown in Fig. 1a is the TEM bright field image of the crystallized Co layer grown under the borosilicate surface oxide on the $Co_{74.26}Fe_{4.74}B_{18.9}Si_{2.1}$ annealed at 400°C for 12 min. The fringe contrast seen within the Co grains suggests existence of planar defects in the lattice, which is further confirmed by the numerous streaks on the {111} diffraction ring in the corresponding electron diffraction pattern of Fig. 1b. The streaks are generated by thin plate-like defects lying on the {111} plane of the Co lattice as the streaks lies tangent to the {111} and {222} rings. The pattern in Fig. 1b shows that the crystallized Co appears to have the face-centered cubic (FCC) structure. In Fig. 1b, the diffraction pattern does not have the {200} peak, which should be present for the FCC lattice. In fact, we have found the missing {200} peak to be the unique signature of the highly faulted Co structure for the composition.

In Fig. 2a and b are the TEM bright field image and the electron diffraction pattern of the $Co_{75.26}Fe_{4.74}B_{18}Si_2$ alloy annealed under same condition. In contrast to Fig. 1a, the TEM image shows a relatively low density of the planar defects on the FCC lattice. Although two samples differ in composition only slightly, the marked difference in microstructure arises as the metalloid concentration is near the critical concentration (as previously determined to be ~20 at.% for B + Si [7]) below which islands of borosilicate and cobalt oxides develop. The porous surface oxides allow the excessive ingress of oxygen to the sub-surface, leading to the internal oxidation of Co. The internal oxidation products can be seen along the grain boundary in Fig. 2a [7]. The difference in the diffraction pattern is also noted in Fig. 2b which is comparatively free of the streaks in agreement with the bright field image. Furthermore, the diffraction pattern has the (200) ring as normal FCC Co in contrast to Fig. 1a, indicating a crystallographic difference between two Co cystallites.

4. Discussion

4.1. Microstructure

The absent {200} peaks in Fig. 1c could have originated from the phase transition of the FCC Co crystals into other FCC derivative structures such as diamond cubic ($Fd3m$) and zinc blende ($F\bar{4}3m$) structures. However, since the diamond cubic lattice involves the directional arrangement of atoms (tetrahedral), the structure is inconsistent with the close packed arrangement of the metallic bonding in the FCC cobalt crystallites.

Chemical analysis of the highly faulted Co grain indicated that the grain was enriched with a substantial amount of oxygen, in which case oxygen atoms could occupy four of the tetrahedral interstices as in the zinc blende lattice in order to produce a weak {200} peak that may not be observable. However, the oxygen atom would be too large to be accommodated in the tetrahedral site. Another possibility is the formation of Co_3O_4 with a spinel structure which would forbid the {200} peak, but the lattice parameter of the oxide is much larger than that of Co. Moreover, none of the above proposed structures would explain the streaks appearing in the diffraction pattern of the faulted Co grains.

Given that it is unlikely that the missing peak in the faulted crystals are due to the phase transition, the absent peak appears to be related to the high density of the planar defects found in the Co crystals. Although the hexagonal closed packed (HCP) structure is the stable form of Co at room temperature, the energy difference between the FCC and HCP for Co is sufficiently small that both structures can be stabilized at room temperature [9]. It is also known that cobalt can undergo a martensitic transformation from FCC to HCP [10]. Thus, it is possible that stacking faults or twins could be created as a result of the allotropic transformation of the cobalt during crystallization. However, the pattern in Fig. 1b does not show any presence of HCP phase; nor does the existence of twinned faults can be responsible for the missing peak.

None of the possible microstructure satisfactorily explains the diffraction pattern of the faulted cobalt; we, therefore, postulate a new structure in which the oxygen atoms randomly substituted on the FCC Co lattice as described in Fig. 3a. The radius of oxygen atom is 0.62 Å which is almost exactly half of that of cobalt atom (1.25 Å) so that two oxygen atoms can occupy single cobalt site on the {111} plane, creating extra {400} planes. The oxygen occupied {400} planes which possess equal scattering amplitude as {200} planes will reduce the {200} diffracted intensity. It is likely that the oxygen atoms will be randomly distributed among the Co {111} planes as shown in Fig. 3b, leading to clusters of oxygen atoms lying on the {111} plane. Such thin cluster will give rise to the streaks found on the diffraction pattern. Thus, the stacking fault arising from the oxygen condensation can explain the absent {200} peak and the streaks in Fig. 1b. The oxygen condensation on the Co {100} actually resembles the Guinier-Preston zone consisting of a plate-like cluster of Cu atoms on the {100} plane of the aluminum matrix in the Al-4%Cu supersaturated solution [11].

The correlation between the observed faults and oxygen in the $Co_{74.26}Fe_{4.74}B_{18.9}Si_{2.1}$ strip is also evidenced as the argon-annealing atmosphere substantially reduced the number of faulted crystallites. TEM bright field image of the $Co_{74.26}Fe_{4.74}B_{18.9}Si_{2.1}$ ribbon annealed in Ar atmosphere is shown in Fig. 4. Highly faulted Co crystallites, similar to Fig. 1a, have been also observed, together with fault-free FCC and HCP Co crystals, after annealing the melt-spun $Co_{80}B_{20}$ alloy at 350°C [12]. Although their annealing was done in vacuum, it is likely that the trapped oxygen in the meta-stable material would induce such stacking faults in localized region.

4.2. Magnetic properties

Shown in Fig. 5 is the typical hysteresis loop of $Co_{75.26-x}Fe_{4.74}(BSi)_{20+x}$ alloy after two-step field annealing in order to be used as a domain wall pinned harmonic sensor [13]. The quality of the sensor is judged

(a)

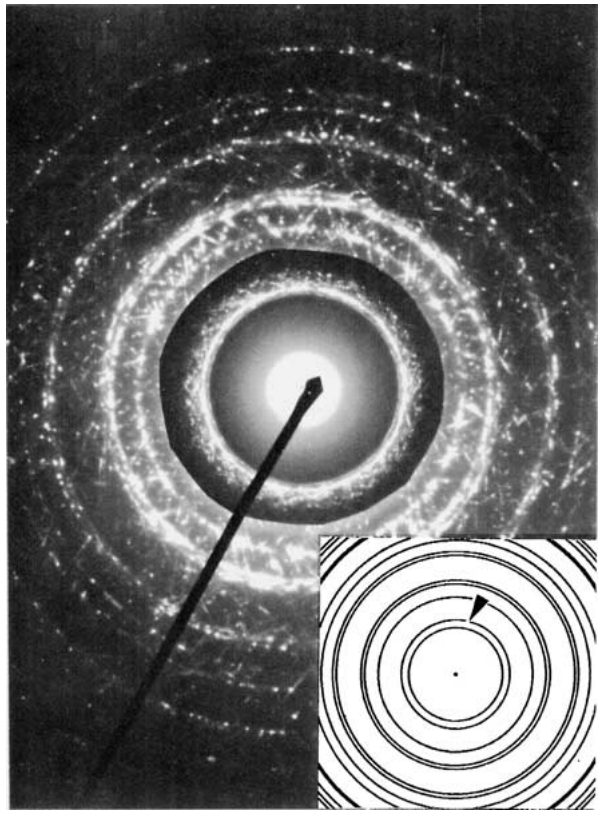

(b)

Figure 1 (a) TEM bright field image of the crystallized Co layer with high density of planar defects in the $Co_{74.26}Fe_{4.74}B_{18.9}Si_{2.1}$ alloy annealed at 400°C for 12 min.; (b) Electron diffraction of the region with the missing {200} ring. The inset shows the diffraction pattern of the normal FCC structure with the {200} peak indicated by the arrow.

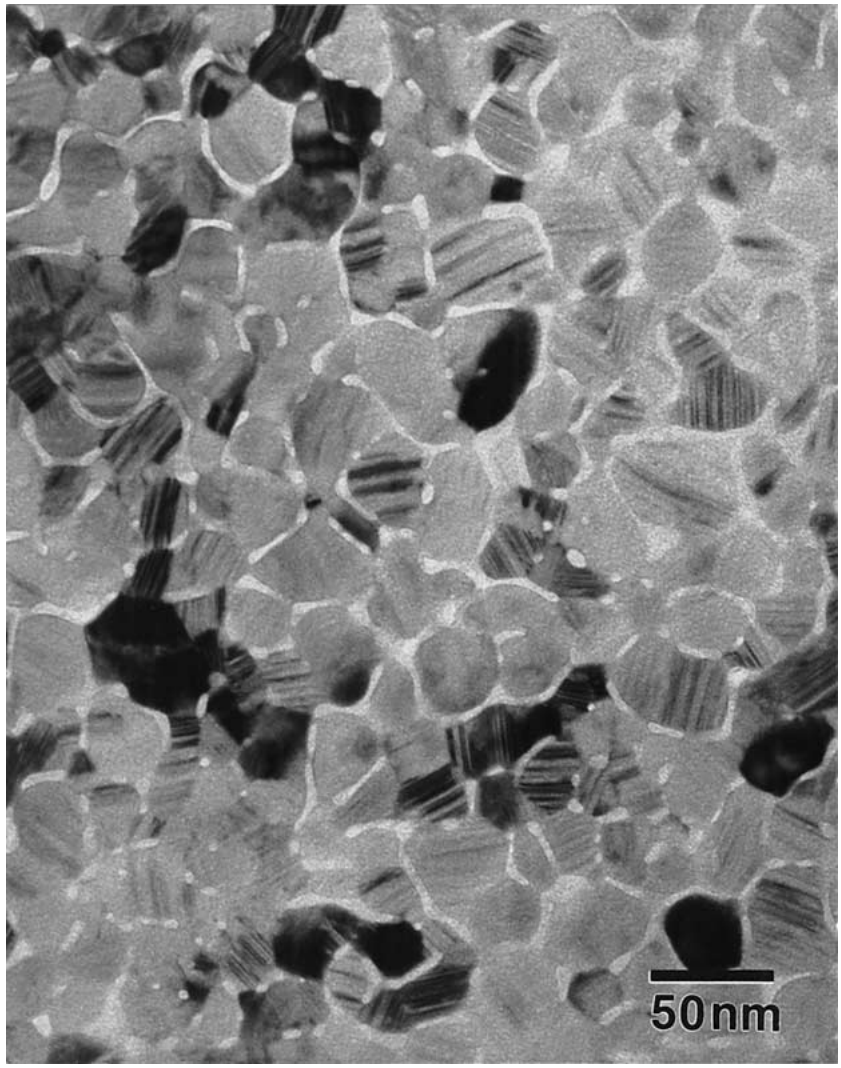

(a)

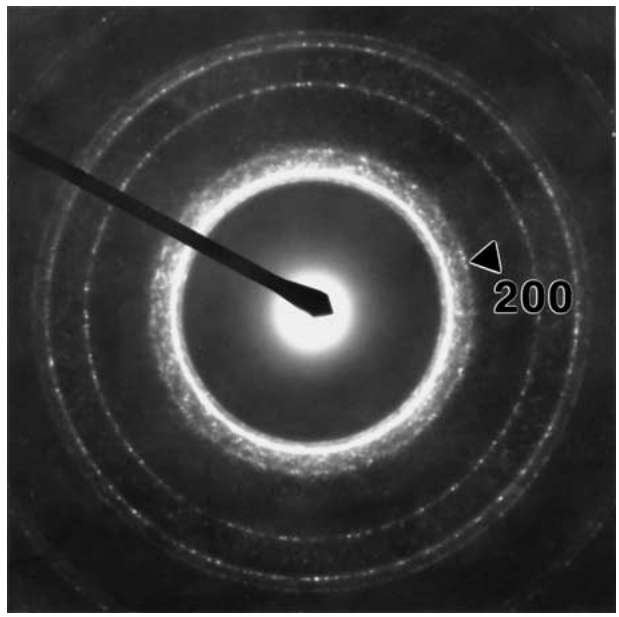

(b)

Figure 2 (a)TEM bright field image of the crystallized Co layer in the $Co_{75.26}Fe_{4.74}B_{18}Si_2$ alloy annealed at 400°C for 12 min.; (b) Electron diffraction of the region.

by having a large H_p, wall pinning threshold which is determined by the nature and density of the domain wall pinned sites.

The strips based on the above two compositions exhibited different magnitude of H_p, suggesting dissimilar domain pinning mechanisms in the material. While the composition, $Co_{74.26}Fe_{4.74}B_{18.9}Si_{2.1}$, had H_p of ∼0.7 Oe, the cast strip in Fig. 2 showed negligible magnitude of the field induced anisotropy. Moreover, when the $Co_{74.26}Fe_{4.74}B_{18.9}Si_{2.1}$ strip was annealed

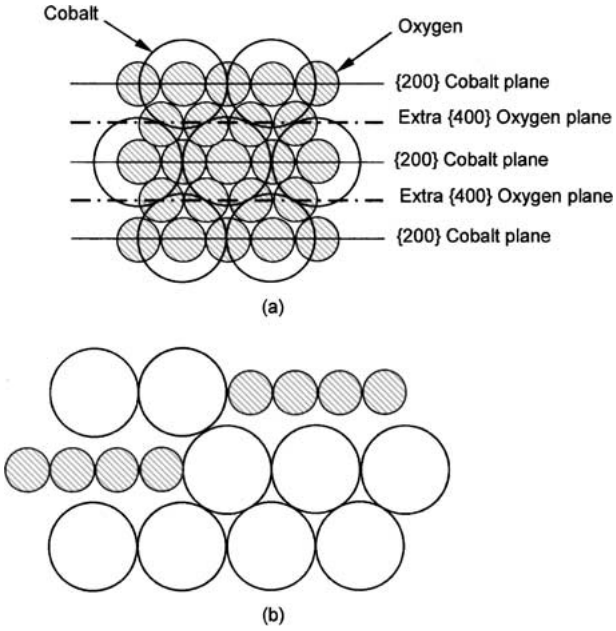

Figure 3 (a) Oxygen layer formed on the Co {111} lattice plane such that two layers of oxygen atoms replaces the single layer of Co; (b) Side-view of random distributed oxygen cluster on the Co {111} planes.

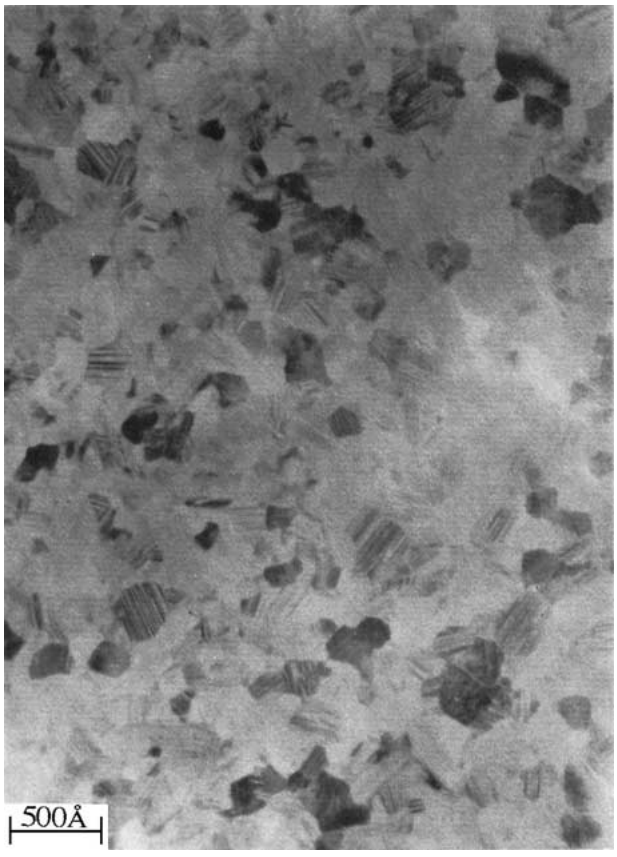

Figure 4 TEM bright field image of the crystallized Co layer in the $Co_{74.26}Fe_{4.74}B_{18.9}Si_{2.1}$ alloy annealed at 400°C for 12 min in Ar atmosphere, showing reduced amount of faults compared to Fig. 1a.

in Ar atmosphere, the material not only showed less faulted crystallites as shown in Fig. 4, but the pinning threshold was noticeably reduced.

Judging from the different magnetic properties, it is likely that the proposed presence of the oxygen in the Co lattice has a strong bearing on the magnetic properties

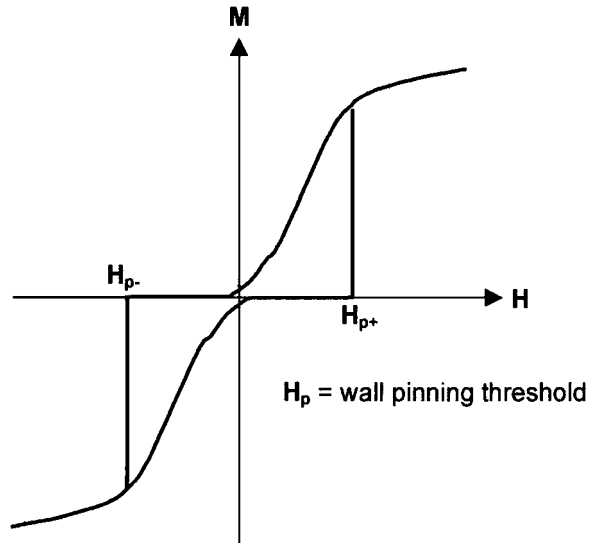

Figure 5 Schematic drawing of the hysteresis loop of the $Co_{75.26-x}Fe_{4.74}(BSi)_{20+x}$ alloy after two-step annealing, showing the wall pinning threshold, H_p.

of the material. It is speculated that the spin arrangement near {111} oxygen plane may resemble that of antiferromagnetic CoO, so as to give the material a localized antiferromagnetic region around the oxygen cluster. Such localized antiferromagnetic region would lead to magnetic anisotropy through exchange coupling between cobalt and the oxygen layer. A strong field induced anisotropy has been reported in the surface oxidized fine Co particles and a similar mechanism has been used to explain the induced anisotropy [14].

5. Conclusion

Electron diffraction of the crystallized Co layer in the amorphous Co-rich alloy revealed that the Co crystallites are highly faulted depending on the composition and the annealing conditions. The fault appears to be a form of stacking fault where the oxygen atoms are randomly substituted in the Co sites, creating a plate-like cluster of oxygen atoms on {111} planes. Such cluster of oxygen atoms would have a strong bearing on the magnetic properties of the material since the oxygen fault appears to closely related to the magnitude of the induced magnetic anisotropy.

Acknowledgement

This work was supported by grant No. R01-1997-00048 from the Basic Research Program of the Korea Science & Engineering Foundation.

References

1. G. E. FISH, *Proceedings of the IEEE* **78**(6) (1990) 947.
2. R. BOLL, H. R. HILZINGER and H. WARLIMENT, in "Glassy Metals: Magneticc, Chemical and Structural Properties," edited by R. Hasegawa (CRC Press, Boca Raton, Florida, 1990) p. 184.
3. H. WARLIMONT, in "Rapidly Quenched Metals," edited by S. Steeb and H. Warlimont (Elsevier Science, Amsterdam, 1985) p. 1599.

4. K. MOHRI, in "Magnetic Properties of Amorphous Metals," edited by A. Hernando, V. Madurga, M. C. Sanchez-Trujillo and M. Vazquez (Elsevier Science, Amsterdam, 1987) p. 3606.
5. G. HERZER and H. R. HILZINGER, in "Magnetic Properties of Amorphous Metals," edited by A. Hernando, V. Madurga, M. C. Sanchez-Trujillo and M. Vazquez (Elsevier Science, Amsterdam, 1987) p. 354.
6. L. HENDERSON, R. C. O'HANDLEY and B. L. AVERBACH, *J. Magn. Magn. Mater*. **87** (1990) 142.
7. C. K. KIM, C. S. YOON, T. Y. BYUN and K. S. HONG, *Oxidation of Metals* **55** (2001) 179.
8. C. K. KIM, W. K. HO and R. C. O'HANDLEY, *IEEE Trans. Magn*. **31**(6) (1995) 4015.
9. R. W. G. WYCKOFF, "Crystal Structures" (Interscience, London, 1960) p. 12.
10. P. HASSEN, "Martensitic Transformations, Physical Metallurgy" (Cambridge University Press, New York, 1978) p. 311.
11. D. A. PORTER and K. E. EASTERLING, "Phase Transformation in Metals and Alloys" (Van Nostrand Reinhold, New York, 1981) p. 291.
12. A. ZERN, I. KLEINSCHROTH, A. GONZALEZ, A. HERNANDO and H. KRONMÜLLER, *J. Appl. Phys*. **85**(11) (1999) 7609.
13. H. KYUNG, C. S. YOON and C. K. KIM, Mat. Sci. Eng. B, submitted.
14. S. CHIKAZUMI, "Physics of Magnetism," edited by S. Chikazumi and S. H. Charap (John Wiley, New York, 1965) p. 359.

Received 17 September 2001
and accepted 30 January 2002